Journal of Catalysis **204,** 219–229 (2001)
doi:10.1006/jcat.2001.3364, available online at http://www.idealibrary.com on IDEAL®

Continuous Semihydrogenation of Phenylacetylene over Amorphous $Pd_{81}Si_{19}$ Alloy in "Supercritical" Carbon Dioxide: Relation between Catalytic Performance and Phase Behavior

Reto Tschan, Roland Wandeler, Michael S. Schneider, Markus M. Schubert, and Alfons Baiker[1]

Laboratory of Technical Chemistry, Swiss Federal Institute of Technology, ETH Hönggerberg-HCI, CH-8093 Zurich, Switzerland

Received May 18, 2001; accepted July 23, 2001

Continuous semihydrogenation of phenylacetylene over an amorphous $Pd_{81}Si_{19}$ catalyst in supercritical CO_2 as a solvent has been studied. The amorphous alloy afforded high selectivity to styrene without catalyst modification, which is usually necessary for high selectivity in "Lindlar-type" hydrogenations. The application of the highly active glassy metal alloy combined with a supercritical solvent afforded efficient operation in a continuous fixed-bed reactor. A single-phase system was found to be an ideal reaction medium for such hydrogenation reactions. Highest conversions and good selectivities were achieved near the transition to a single-phase mixture, where mass transport is enhanced by elimination of the gas–liquid interface. In order to reach complete miscibility of the reactants in CO_2 at moderate pressure, both temperature and hydrogen excess had to be kept low. The phase behavior was monitored by online video imaging. Consideration of the phase behavior was found to be indispensable for assessing single-phase conditions. A binary fluid-phase diagram is shown to serve as a good guide to understanding the multicomponent behavior.

Key Words: **phenylacetylene; phenylethyne; styrene; selective hydrogenation; supercritical carbon dioxide; semihydrogenation of triple bonds; metallic glasses; phase behavior.**

INTRODUCTION

Favorable application of a highly active heterogeneous catalyst in the liquid phase is often impaired by inherently slow mass transfer, resulting in nonoptimal use of such catalysts. Slow interface mass transfer can be enhanced when reactions are carried out in supercritical (sc) media. In this work we demonstrate the beneficial application of a highly active glassy metal catalyst in combination with a "supercritical" solvent, using the semihydrogenation of phenylacetylene (PA) to styrene (ST) (Scheme 1) over an amorphous $Pd_{81}Si_{19}$ alloy in supercritical carbon dioxide as an example.

The use of supercritical fluids in catalysis has been the focus of several recent reviews (1–5). Application of supercritical fluids offers not only a favorable combination of heat and mass transfer but also other advantages such as process intensification or easy separation of solvent and product/reactants (4). A supercritical fluid (SCF) of particular interest in chemical technology is CO_2 (6, 7). Carbon dioxide is nonflammable, environmentally benign, and readily available at low cost compared to most other standard solvents. Furthermore, the supercritical state of carbon dioxide is relatively easily accessible ($T_c = 30.9°C$, $p_c = 73.8$ bar) (8) and offers moderate density ($\rho_c = 0.47 \times 10^3$ kg m^{-3}) (8) and solvent power. CO_2 is particularly suitable as a solvent for numerous continuous hydrogenations (9).

Polymerized monovinyl aromatic compounds, such as polystyrene, are a widely used class of thermoplastics (10). A common way to manufacture the ST monomers is by ethylation of benzene to form ethylbenzene (EB), which is subsequently dehydrogenated to styrene. The product stream from the dehydrogenation unit contains ST, as well as EB and phenylacetylene (PA), which is formed by overdehydrogenation of EB (10, 11). The presence of PA during the polymerization process has detrimental effects on the molecular weight of the polymer and on the polymerization rate (10, 12). While unreacted EB from the dehydrogenation step can easily be removed by distillation, PA cannot be removed by conventional separation processes and has to be hydrogenated to styrene (Scheme 1) (10). A problem, however, is the consecutive reaction of styrene to EB (10, 11).

Previous studies showed that amorphous metal alloys ("metallic glasses"), such as $Pd_{81}Si_{19}$, are particularly suitable for such semihydrogenation reactions compared to, e.g., conventional supported catalysts (13). Preparation and structural and catalytic properties of metallic glasses have been covered in several reviews (14–16).

Here we show that the continuous semihydrogenation of phenylacetylene over an amorphous $Pd_{81}Si_{19}$ metal alloy catalyst in "sc" CO_2 affords high conversions and selectivities. High selectivity to styrene was achieved without the use of modifiers, which are usually employed to increase selectivity in "Lindlar-type" semihydrogenations (17, 18).

[1] To whom correspondence should be addressed. E-mail: baiker@tech.chem.ethz.ch. Fax: +41 (1) 632 11 63.

0021-9517/01 $35.00

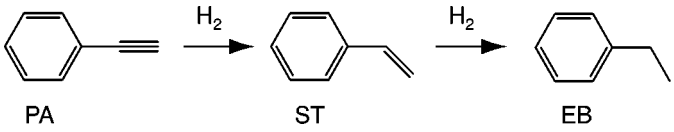

SCHEME 1. Hydrogenation of phenylacetylene (PA) to styrene (ST) and the consecutive hydrogenation to ethylbenzene (EB).

The phase behavior and its influence on the reaction are studied in detail, demonstrating that the highest styrene yields are achieved near the transition to a "supercritical" single-phase system. From the results it emerges that the combination of a highly active $Pd_{81}Si_{19}$ catalyst with a "supercritical" solvent is excellently suited for "Lindlar-type" hydrogenations.

EXPERIMENTAL

Materials

Styrene (puriss., stabilized with 0.005% 4-*tert*-butyl catechol) and phenylacetylene (purum) were obtained from Fluka AG. Carbon dioxide (99.99%) and hydrogen (99.99%) were used as purchased.

Th $Pd_{81}Si_{19}$ amorphous metal alloy, used as catalyst material, supplied by Degussa AG, was produced by melt spinning. For application the melt spun ribbons were ground to flakes with a diameter ca. 0.1–1 mm under liquid nitrogen to avoid partial crystallization of the material due to the mechanical impact. The ground material possessed a Brunauer–Emmet–Teller (BET) surface area of 0.01 $m^2\ g^{-1}$, as determined by krypton adsorption measurements.

Catalyst Characterization

X-ray diffraction (XRD) patterns were recorded on a Siemens D5000 $\theta - 2\theta$ diffractometer, using Ni-filtered CuK_α radiation (45 kV, 35 mA) in step mode with a step size of 0.01° and 0.3 s.

Thermal analysis (TA) experiments were carried out on a Netzsch STA 409 thermoanalyzer coupled to a QMG 420 mass spectrometer (Balzers) by a stainless-steel capillary heated to 200°C. The heating rate was 10 K min^{-1} and the flow rate of the carrier gas (Ar) 50 ml min^{-1}. In the DSC measurement the empty Pt crucible was used as reference.

The X-ray photoelectron spectroscopy (XPS) measurements were performed at room temperature using a Leybold Heraeus LHS11 apparatus equipped with a Mg source (1253.6 eV) and operating at 240 W. Quantification was performed using the sensitivity factors reported by Wagner *et al.* (19).

Scanning electron micrographs (SEM) were acquired on a Hitachi S-900 "in-lens" field emission scanning electron microscope operated at 5 or 30 kV.

Specific surface areas were evaluated using the BET method on a Micromeritics ASAP 2010 instrument using krypton as adsorbing gas at 77 K.

Continuous High-Pressure Reactor System

The computer-controlled continuous flow stainless-steel reactor system was designed for pressures up to 280 bar and temperatures up to 200°C. The apparatus, which essentially consisted of a dosing system for reactants and solvent (CO_2), a tubular reactor, pressure and temperature control, automatic sampling, and an analytical part, is shown schematically in Fig. 1. The carbon dioxide flow

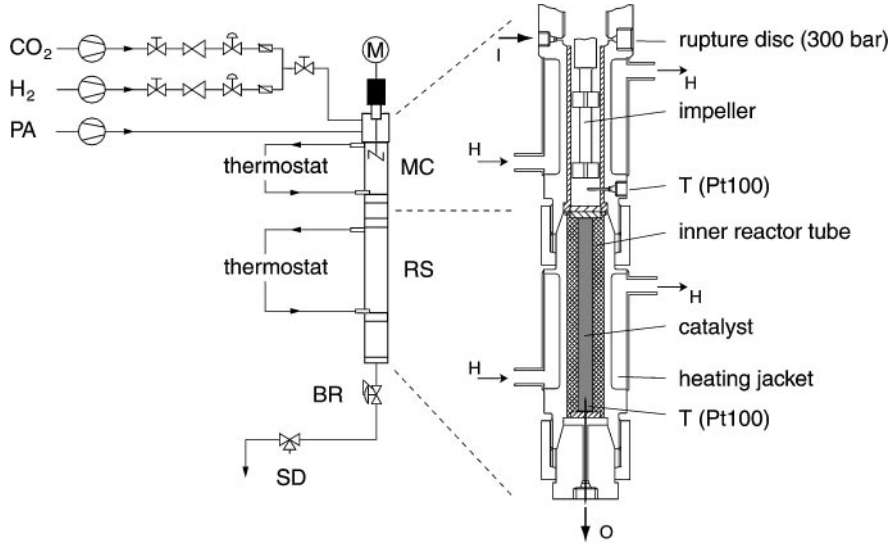

FIG. 1. Schematic presentation of the high-pressure continuous fixed-bed reactor system. MC, mixing chamber; RS, reactor section; BR, back-pressure regulator; SD, sampling device; I, inlets; O, outlets; H, heat transfer oil.

was controlled by a combination of a flow meter (HI-Tec Bronkhorst; El-Flow) and a needle valve (Kämmer; 80037-IP). The hydrogen flow was controlled by a flow meter/controller (HI-Tec Bronkhorst; El-Flow). Liquid reactants were being fed into the system through a HPLC pump (Jasco PU-980). All feed streams were combined in a mixing chamber (MC), equipped with a mechanical Teflon stirrer, before entering the vertically mounted reactor section (RS; ID = 25 mm; length = 125 mm). For safety reasons and for better handling the reactor section consisted of two concentric stainless-steel tubes. The inner tube (ID = 5 mm), containing the catalyst, was inserted into the outer tube and sealed by O-rings at its front end to avoid by-passing. The catalyst was fixed in the reactor tube by quartz wool plugs. Temperature in the mixing chamber and in the reactor was measured via Pt100 resistance temperature detectors and was controlled by two thermostats (ToolTemp TT-220). Pressure was controlled by a backpressure regulator (Tescom Series 26–1700; BR), located just after the reactor section. A strip heater was wrapped around the backpressure regulator to prevent the valve from freezing due to the expansion of carbon dioxide. Pressure measurement was accomplished by pressure transmitters (Keller; PA-23/8465-400). Sample volumes (ca. 3 ml) were branched off from the product stream at intervals of 30–60 min by a computer-controlled three-way valve placed just after the backpressure regulator (expansion to ambient conditions) and directed to an automatic sampling device (SD). The complete setup was controlled by an autonomic process computer (Eurotherm). Direct logical commands (e.g., controlling of valves), display functions, and data acquisition routines were programmed via the Intellution Fix software package on a personal computer.

Analysis was established by injecting the samples into a gas chromatograph (GC) (HP 6890 series) by an autosampling device (HP 7683 series) after dilution with 1-octanol. The GC was equipped with a split/splitless injector (sample volume 1 μl), a capillary column (Macherey & Nagel Permabond CW20M; 0.25 μm, 30 m, 0.25 mm), and a flame-ionization detector (FID). Helium was used as carrier gas. Concentrations of PA, ST, and EB, which were previously calibrated by samples of known composition, were determined on the basis of area%. When a mixture of PA–ST was fed to the reactor, selectivity was defined as $[PA_0 - PA]/([PA_0 - PA] + [EB])$, thus taking into account the undesired hydrogenation of ST to EB.

Catalytic Studies

Carbon dioxide flow and reactant flow (PA or PA–ST mixture, resp.) were held constant at 180 and 10 g h^{-1}, respectively, throughout all experiments. Parameter studies were carried out with 0.25 g (*p* and *T* experiments) and 1.0 g (H_2 experiments) amorphous $Pd_{81}Si_{19}$ catalyst, resulting in catalyst bed lengths of approximately 4 and 15 mm (plus quartz wool plugs), respectively. Steady state was reached after ca. 90 min; all catalytic data were recorded after 2–3 h on-stream, except where noted otherwise.

Phase Behavior Studies

The phase behavior of the system under reaction conditions was investigated in a computer-controlled high-pressure view cell of variable volume (23–63 ml), equipped with online digital video imaging and recording. The system has been described elsewhere (20). The magnetically stirred cell consisted of a horizontal cylinder equipped with a sapphire window covering the entire diameter and an opposite, horizontally moving piston equipped with another sapphire window for illumination of the system. This setup allowed observation of even minor volumes of gaseous and liquid phases.

Note that the widely used term *supercritical* is deprived of any meaning in multicomponent systems, since phase separation is still possible under conditions beyond the mixture critical point ("retrograde condensation" (21, 22)) or the critical points of the pure components ("gas–gas immiscibility" (22)). For convenience, the term "supercritical" is used here in quotes for a dense fluid phase at temperatures exceeding its mixture critical point, irrespective of further liquid phases present.

RESULTS

Preliminary experiments on the hydrogenation of pure PA over the amorphous $Pd_{81}Si_{19}$ catalyst revealed that high selectivity to ST (as high as 96%) was achieved and remained virtually constant even for the highest conversion degrees (Fig. 2). This behavior can be explained by two factors, namely, the low and decreasing H_2 concentration with

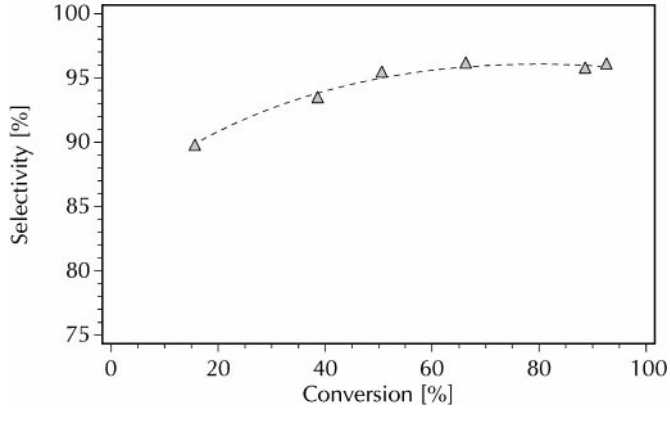

FIG. 2. Selectivity vs conversion for the hydrogenation of phenylacetylene over amorphous $Pd_{81}Si_{19}$, observed by variation of the catalyst mass (0.2–4 g). Reaction conditions: $T = 55°C$; $p = 127$ bar; PA flow = 10 g h^{-1}; $CO_2 : PA : H_2$ molar ratio = 40 : 1 : 2.

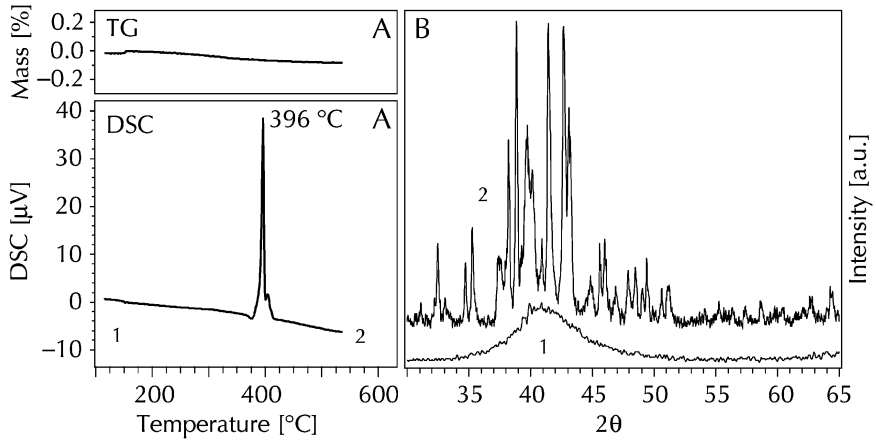

FIG. 3. (A) Thermal analysis (TG and DSC) of amorphous $Pd_{81}Si_{91}$ alloy. Crystallization occurred above 390°C in an inert gas atmosphere (Ar) and at a heating rate of 10 K min^{-1}. (B) XRD pattern before (1) and after (2) crystallization.

conversion and the intrinsic high triple bond hydrogenation selectivity of the metallic glass. In the following, experiments were performed with a PA–ST mixture with a 1 : 9 molar ratio. In such a system, the selectivity should be subject to greater changes with variation of reaction parameters. Furthermore, a mixture containing low concentrations of PA in ST is more closely related to the industrially interesting application of styrene purification (10, 12, 23, 24). The experimental results are divided into catalyst properties, phase behavior, and catalytic studies. The latter two will be interrelated under Discussion.

Catalyst Properties

XRD analysis of the $Pd_{81}Si_{19}$ used in the catalytic tests confirmed that the material was amorphous; that is, no indication of any long-range ordering of the constituents was observed (Fig. 3B, pattern 1). Crystallization occurred above 390°C in an inert gas atmosphere, as shown by thermal analysis (DSC; Fig. 3A). Pattern 2 in Fig. 3B shows the XRD pattern after the sample was heated to ca. 550°C. Distinct reflections due to the crystalline structure of the material are discernible. Scanning electron microcopy (SEM) revealed a rather rough surface containing areas with a "spike"-like structure (Fig. 4). The surface composition of the amorphous alloy, as analyzed by XPS, indicated an O : Si : Pd ratio of roughly 75 : 15 : 10 (at %), revealing a significant enrichment of Si in the surface region compared to the bulk composition. The binding energies were 103.1 eV for Si 2p and 335.6 eV for Pd $3d_{5/2}$ compensating sample charging with C 1s at 284.8 eV as internal standard. A detailed study of the effect of various pretreatment methods on the surface composition of $Pd_{81}Si_{19}$ using ISS and XPS was published by Noack *et al.* (25). The observations of silicon enrichment on the surface are in agreement with their findings.

Phase Behavior Studies

The reaction mixture CO_2/PA–ST/H_2 exhibited diverse phase behavior in the parameter range examined (20–85°C, pressure up to 180 bar), as illustrated in Fig. 5. The number, nature, and composition of the mutually saturated phases depended strongly on temperature and pressure (Fig. 6).

At 20°C and low pressure, the system consisted of a liquid PA–ST-rich phase in equilibrium with a gaseous CO_2-rich phase. An increase in pressure resulted in an increase of the liquid level, i.e., of the homogeneous liquid PA–ST/CO_2-rich phase in equilibrium with a vapor phase. The system turned into a liquid PA–ST/CO_2/H_2 single phase at pressures above ca. 125 bar.

In the temperature range 30–45°C, the system exhibited similar behavior at low pressure, i.e., an equilibrium of a PA–ST-rich liquid phase with a CO_2-rich gaseous phase. At intermediate pressure (ca. 30–100 bar), however, the system revealed partial immiscibility of liquid PA–ST and CO_2. This led to a three-phase liquid–liquid–vapor (LLV) equilibrium between a liquid PA–ST-rich phase, a liquid CO_2-rich phase, and a gaseous CO_2/H_2-rich phase. A further increase in pressure resulted in a steady decrease of the amount of liquid PA–ST-rich phase in this LLV equilibrium, and finally in an equilibrium of a homogeneous liquid PA–ST/CO_2-rich phase and a vapor phase at pressures above ca. 95 bar for 35°C. At pressures exceeding ca. 135 bar, the system again exhibited liquid PA–ST/CO_2/H_2 single-phase behavior.

The appearance of a three-phase liquid–liquid–vapor equilibrium was limited to temperatures below ca. 47°C. It ended with the disappearance of the liquid CO_2-rich phase, leaving a gaseous ("sc") CO_2-rich phase of almost similar density (see Fig. 5, snapshot C) in equilibrium with the PA–ST-rich liquid phase. The similarity in density of the two CO_2-rich phases marks the proximity to a critical point

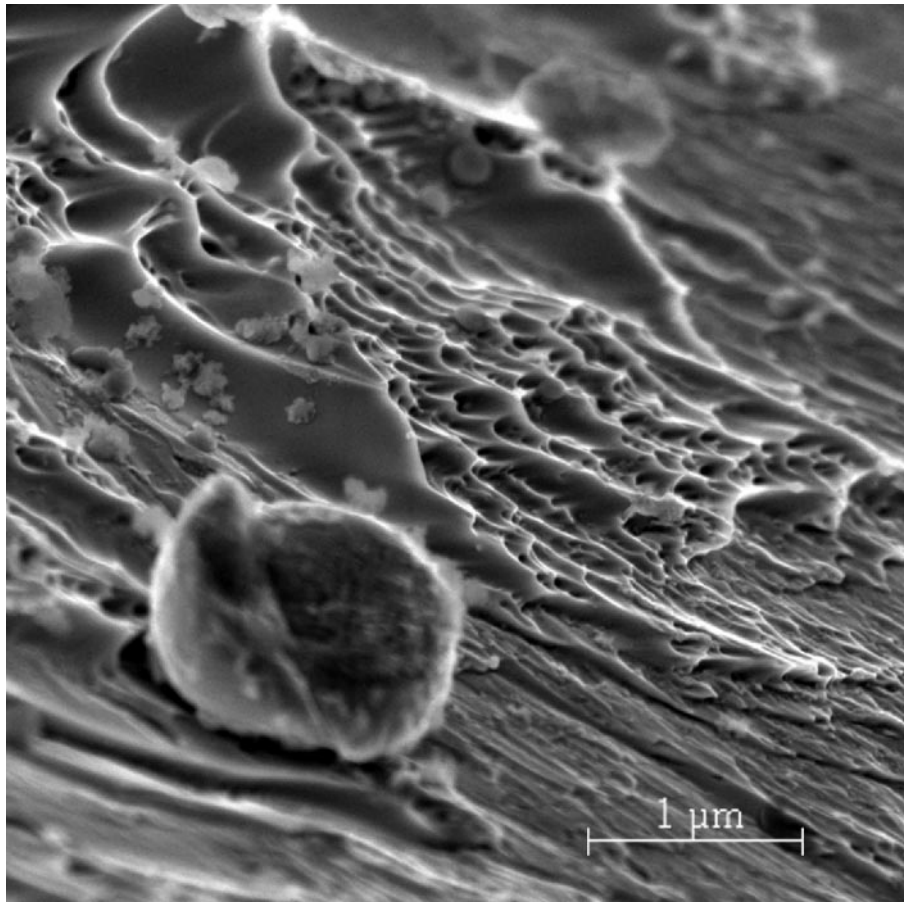

FIG. 4. Scanning electron micrograph of $Pd_{81}Si_{19}$ amorphous metal alloy flakes used as catalyst. Image was acquired on a Hitachi S-900 "in-lens" field emission scanning electron microscope operated at 5 kV.

(and probably also to the upper critical endpoint of the LLV equilibrium).

At temperatures beyond the coexistence of CO_2-rich phases, the system exhibited an equilibrium of a liquid PA–ST-rich phase and a sc CO_2-rich phase at low pressure. The amount of liquid phase decreased with increasing pressure in the range exceeding 90 bar, resulting again in a single-phase system at high pressures. This sc single-phase region was fully established at pressures above 135 and 180 bar for 55 and 70°C, respectively (Fig. 7).

Catalytic Studies

Figure 8 shows the effect of variation of pressure on the reaction in the range 50–200 bar and at a constant reaction temperature of 55°C. The conversion increased strongly above 80 bar, reached a maximum at 130 bar, and remained almost constant when pressure was further increased. Initially, selectivity showed an opposite tendency and decreased most strongly in the range 80–130 bar. At higher pressure and almost constant conversion, however, selectivity was further reduced. As a consequence, the achieved styrene purity, i.e., ST content in the product steam, reached its optimum at a pressure of ca. 130 bar.

Figure 9 illustrates how PA conversion increased steadily from 65 to 90% with increasing temperature in the range 55–85°C and at a constant pressure of 127 bar. The observed selectivity reached a maximum at approximately 65°C and decreased again at higher temperatures. Superposition of these trends resulted in almost constant ST purity over the investigated temperature range.

In Fig. 10 the hydrogen concentration was varied from a $PA:H_2$ ratio of 1:10 to 1:80. Higher overall conversion and lower selectivity, compared to those in the previous figures, are explained with a larger amount of catalyst. With increasing concentration of hydrogen, selectivity decreased from 79 to 62%, accompanied by a small increase in conversion from 90 to 95%. The highest styrene purity was achieved at the lowest hydrogen excess. Unfortunately, due to technical limitations of the experimental setup, the concentration of hydrogen could not be further reduced.

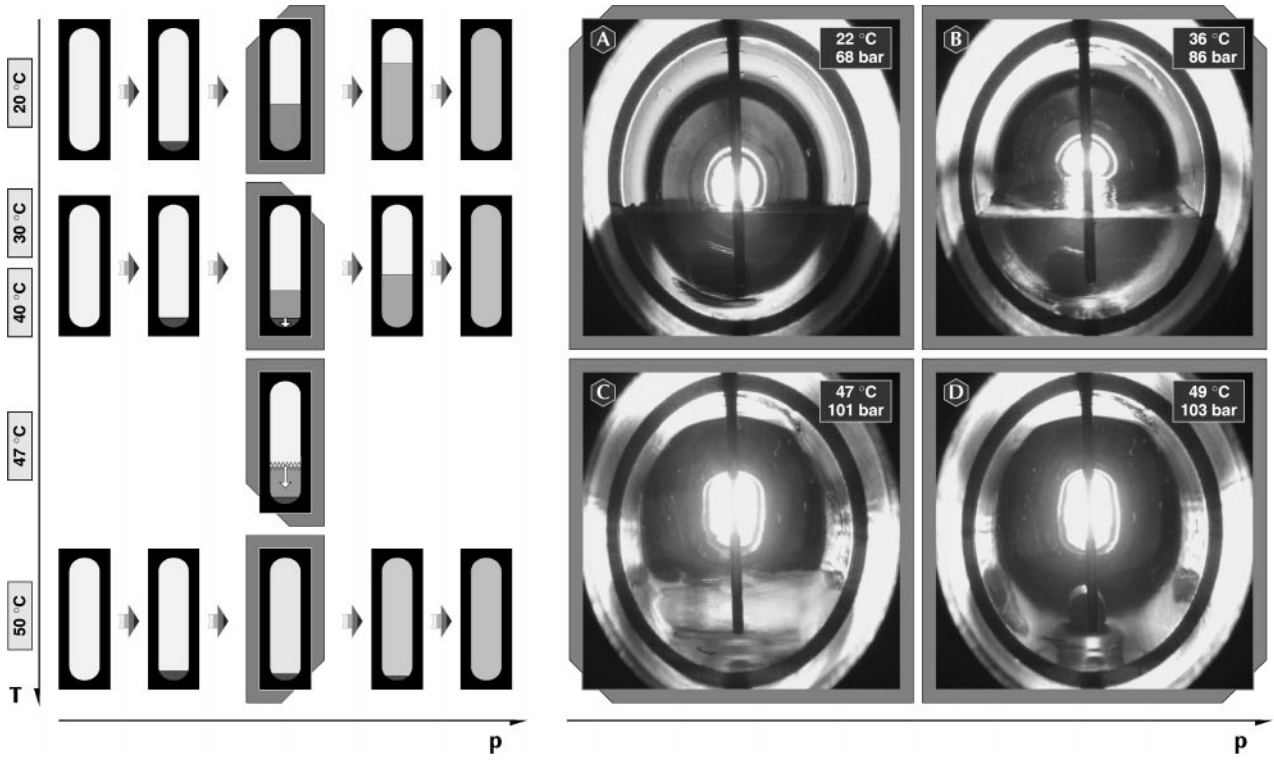

FIG. 5. Phase behavior in the system CO_2 : (PA : ST) : H_2 with a molar ratio of 400 : (1 : 9) : 10 as a function of pressure and temperature. The phase transitions in the shaded boxes are illustrated (from top to bottom) by the snapshots A–D. 20°C: Fully miscible liquid PA–ST and CO_2 lead to a "conventional" transition from a gaseous system at low pressures to a liquid one at higher pressures by way of a two-phase region. 30–40°C: Only partially miscible liquid PA–ST and CO_2; condensation of a PA–ST-rich liquid phase at low pressures and an additional CO_2-rich liquid phase as pressure is increased, leading to a liquid–liquid–vapor equilibrium. A further increase in pressure leads to a two-phase equilibrium of CO_2-rich phases, and finally to a single liquid phase. 47°C: Upper temperature end of the three-phase liquid–liquid equilibrium area: disappearance of the liquid CO_2-rich phase in the vicinity of a critical point of the two CO_2-rich phases. 50°C: Condensation of a PA–ST-rich liquid phase in equilibrium with a gas-like "sc" CO_2-rich phase; transition to a single-phase system with increasing pressure. General features of snapshots: The bright round spot at the opposite end of the cell is the sapphire window used for illumination. The outer white circle is caused by reflection of light at the outer flange of the sapphire window. The vertical thermocouple and PTFE magnetic stirrer at the bottom of the cell are visible.

DISCUSSION

In the following we first discuss the phase behavior, which subsequently we relate to the catalytic studies.

Phase Behavior

The reaction system exhibited diverse phase behavior in the parameter range considered. Liquid PA–ST and CO_2 were only partially miscible at temperatures exceeding ca. 25°C, while being fully miscible at lower temperatures (verified down to 15°C) at the employed molar ratio.

The solubility of PA and ST, respectively, in the CO_2-rich phase is expected to depend mainly on the density of the latter in the temperature range investigated (26). As can be seen in Fig. 6, complete dissolution of PA–ST in the CO_2-rich phase occurred only for densities exceeding ca. 550 kg m^{-3}, resulting in a saturated CO_2-rich phase at this threshold value. In the temperature range 25–45°C and at pressures where liquid and gaseous CO_2-rich phases coexist, the liquid CO_2-rich phase apparently has densities lower than 550 kg m^{-3}. The lower density of the liquid CO_2-rich phase explains the partial immiscibility of liquid CO_2 and PA–ST and thus the appearance of a three-phase liquid–liquid–vapor equilibrium under these cnditions. With high enough pressures in this temperature range, however, the density of liquid CO_2 again exceeds the threshold value of 550 kg m^{-3}, leading to a miscible PA–ST/CO_2 system in equilibrium with a vapor phase at first and subsequently to a single-phase system. Note that the development of the density of the CO_2-rich phase in the reaction system with temperature and pressure is analogous to the behavior of the liquid-phase density in the fluid two-phase region for pure CO_2.

The pressure required for exceeding the threshold density of 550 kg m^{-3}—and thus for complete solubility of PA–ST in the CO_2-rich phase—increased considerably with temperature (see Fig. 6). Note that this pressure increase is more pronounced in the presence of H_2 than in pure CO_2 or a system of CO_2/PA–ST. This effect is explained by the

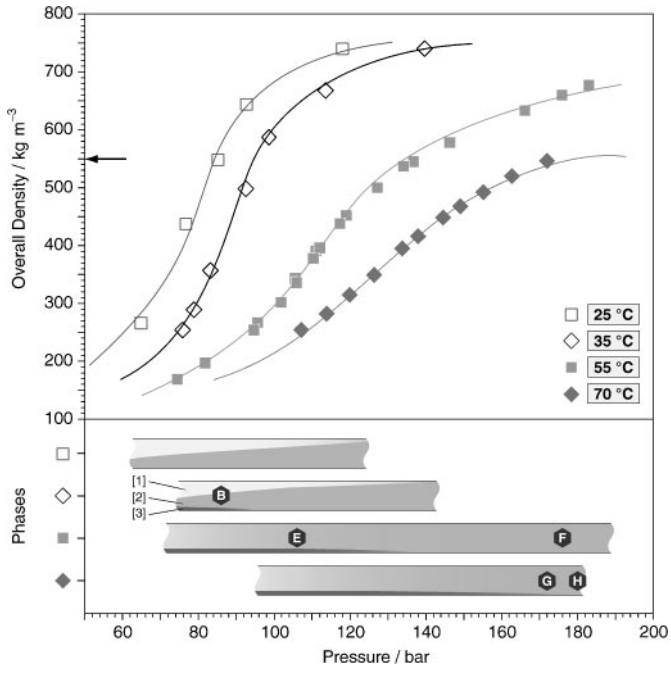

FIG. 6. Influence of pressure on the overall density and phase behavior of the reaction mixture for 25°C (white squares), 35°C (white diamonds), 55°C (gray squares), and 70°C (gray diamonds). CO_2 : (PA : ST) : $H_2 = 400 : (1 : 9) : 10$. Phases: [1] gaseous, CO_2/H_2-rich phase; [2] dense fluid, CO_2-rich phase; [3] liquid, PA–ST-rich phase. Arrow on *y* axis indicates the density required to reach the single-phase region. Note the significant increase of pressure required to reach this density at increased temperatures. The labeled hexagons correspond to the snapshots in Figs. 5 and 7.

strong nonideal gas behavior of hydrogen in high-pressure mixtures.

As illustrated in Fig. 5, the phase behavior of the hydrogenation reaction mixture is very distinct from that of the pure solvent CO_2. Although some of the qualities of sc CO_2, such as density, are still reflected in the phase properties of the mixture, presumption of a phase behavior similar to that of pure CO_2 would lead to major flaws in the interpretation of reaction data. Bearing the critical parameters of CO_2 in mind, it could be tempting to attribute the beginning of the rise in PA conversion with pressure (Fig. 8) to a change in phase behavior at the critical pressure of pure CO_2. Indeed, graphs of reaction data with indicated critical pressure or temperature of the pure solvent are quite common in the literature. This study corroborates that such uncritical presumption of a phase behavior parallel to that of the pure solvent may be fatal in a scientific interpretation of high-pressure reactions. A detailed consideration of the changes in number, nature, and composition of phases in the parameter range explored is indispensable.

The phase behavior of the hydrogenation reaction mixture can be understood in terms of partial immiscibility of liquid PA–ST and CO_2-rich phases at higher temperatures, interfering with the gas–liquid critical line of the CO_2-rich phases. It can be approached in the parameter range considered by using the high-temperature section of a binary fluid-phase diagram of type IV or V as a model (classification of binary mixtures according to Scott and van Konynenburg (27, 28)). Binary mixtures conforming to types IV and V reveal complete miscibility of liquid phases at intermediate temperatures with the presence of a region of liquid–liquid immiscibility up to higher temperatures, and thus interference with the gas–liquid critical line. Type IV behavior additionally exhibits low-temperature liquid–liquid immiscibility. Figure 11 shows a qualitative axonometry of the higher temperature section of phase diagrams found in types IV and V binary mixtures. The isopleth at composition x_m in this diagram shows the same phase topology as was found in the hydrogenation reaction mixture—apart, of course, from a higher degree of freedom for the three-phase equilibrium found in the multi-component mixture examined. The change in phase behavior with pressure in the temperature range 20–70°C (see Fig. 5) may be well approximated by that of the binary model, as illustrated in Fig. 12.

The binary mixture model embeds the experimentally observed phase behavior into a broader context. It

FIG. 7. Interlaced video image of the view-cell showing the transition from a two-phase equilibrium of a liquid PA–ST-rich phase and a "sc" CO_2-rich phase (E, G) to a "sc" single phase (F, H) for ca. 55 and 70°C, respectively. Note that whereas (E) shows the two-phase equilibrium at densities remote from the transition to a single phase for 54°C, (G) corresponds to the two-phase equilibrium in the vicinity of the change to a single phase at 70°C, as is evident from the levels of the PA–ST-rich liquid phase. For explanation of general features cf. Fig. 5.

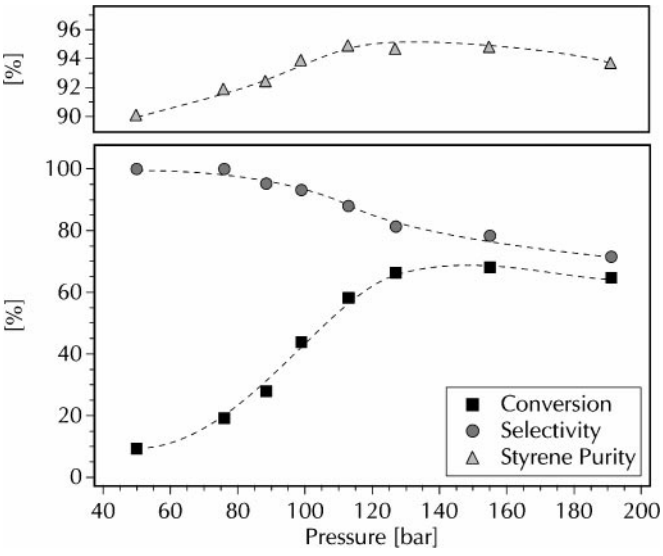

FIG. 8. Influence of pressure on conversion, selectivity, and styrene purity in the semihydrogenation of phenylacetylene over $Pd_{81}Si_{19}$. Reaction conditions: $T = 55°C$, PA–ST flow = 10 g h^{-1}, CO_2 : (PA : ST) : H_2 molar ratio = 400 : (1 : 9) : 10, 0.25 g amorphous $Pd_{81}Si_{19}$ catalyst.

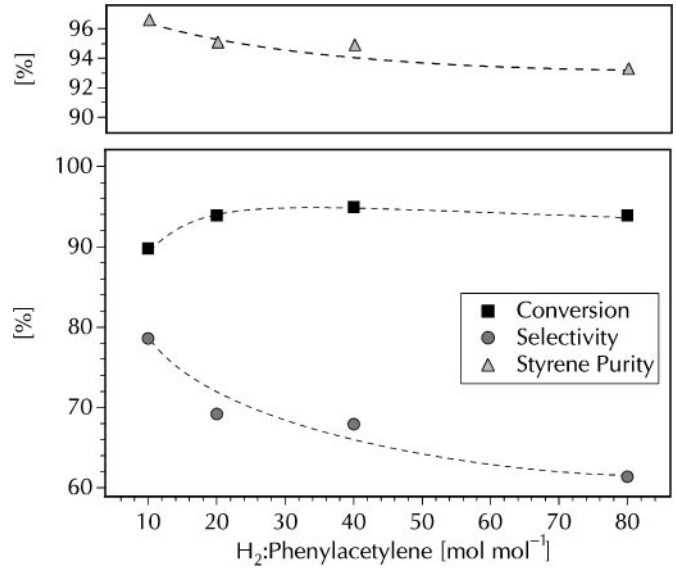

FIG. 10. Influence of hydrogen concentration on conversion, selectivity, and styrene purity in the semihydrogenation of phenylacetylene over $Pd_{81}Si_{19}$. Reaction conditions: $T = 55°C$, $p = 127$ bar, PA–ST flow = 10 g h^{-1}, CO_2 : (PA : ST) molar ratio = 400 : (1 : 9), 1.0 g amorphous $Pd_{81}Si_{19}$ catalyst.

facilitates the qualitative understanding of the multicomponent phenomena observed. Furthermore, it provides a practical basis for extrapolation of the observed phase behavior to other temperatures and pressures—a prerequisite for the rational design of further experiments—especially when the accuracy of the model is weighed against the complexity thus introduced.

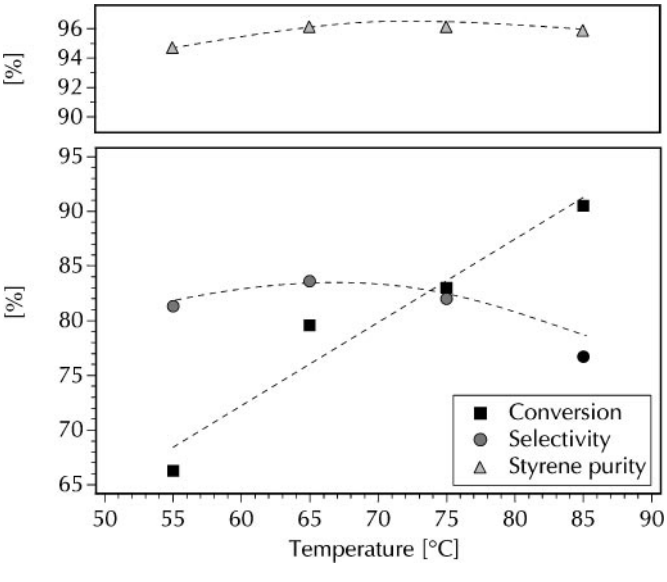

FIG. 9. Influence of temperature on conversion, selectivity, and styrene purity in the semihydrogenation of phenylacetylene over $Pd_{81}Si_{19}$. Reaction conditions: $p = 127$ bar, PA–ST flow = 10 g h^{-1}, CO_2 : (PA : ST) : H_2 molar ratio = 400 : (1 : 9) : 10, 0.25 g amorphous $Pd_{81}Si_{19}$ catalyst.

Relation of Catalytic Studies and Phase Behavior

In the temperature and pressure ranges considered for continuous hydrogenation (55–85°C, 50–180 bar), the reaction mixture exists in a two-phase equilibrium of a PA–ST-rich liquid phase with a sc CO_2-rich phase, transforming into a single-phase system at higher pressures, as described earlier. Note that although the number and nature of phases show a relatively simple phase diagram topology in this parameter range, the composition of coexisting phases changes gradually with temperature, pressure, and H_2 concentration. The observed variations in reaction rate and selectivity with pressure, temperature, and composition were interpreted on the basis of this phase behavior.

In the temperature range examined, PA is predominantly present in a liquid PA–ST-rich phase at low overall densities. Mass transport limitations of H_2 in this liquid phase render it a nonideal medium for (fast) hydrogenation reactions. These factors account for the low conversion of PA observed at low pressure (Fig. 8). With increasing overall density (i.e., pressure) at a constant temperature, two major effects must be considered: (i) the concentration of PA in the CO_2-rich phase steadily increased, slowly shifting the predominant locus of PA hydrogenation from the PA-rich liquid phase to the "sc" CO_2-rich phase; (ii) molecular concentration of reactants and thus the residence time in the catalyst bed increased, this being of relevance since positive reaction orders were determined for all reactants in the hydrogenation of phenylacetylene over platinum metal complexes (29). Accordingly, conversion of PA is expected

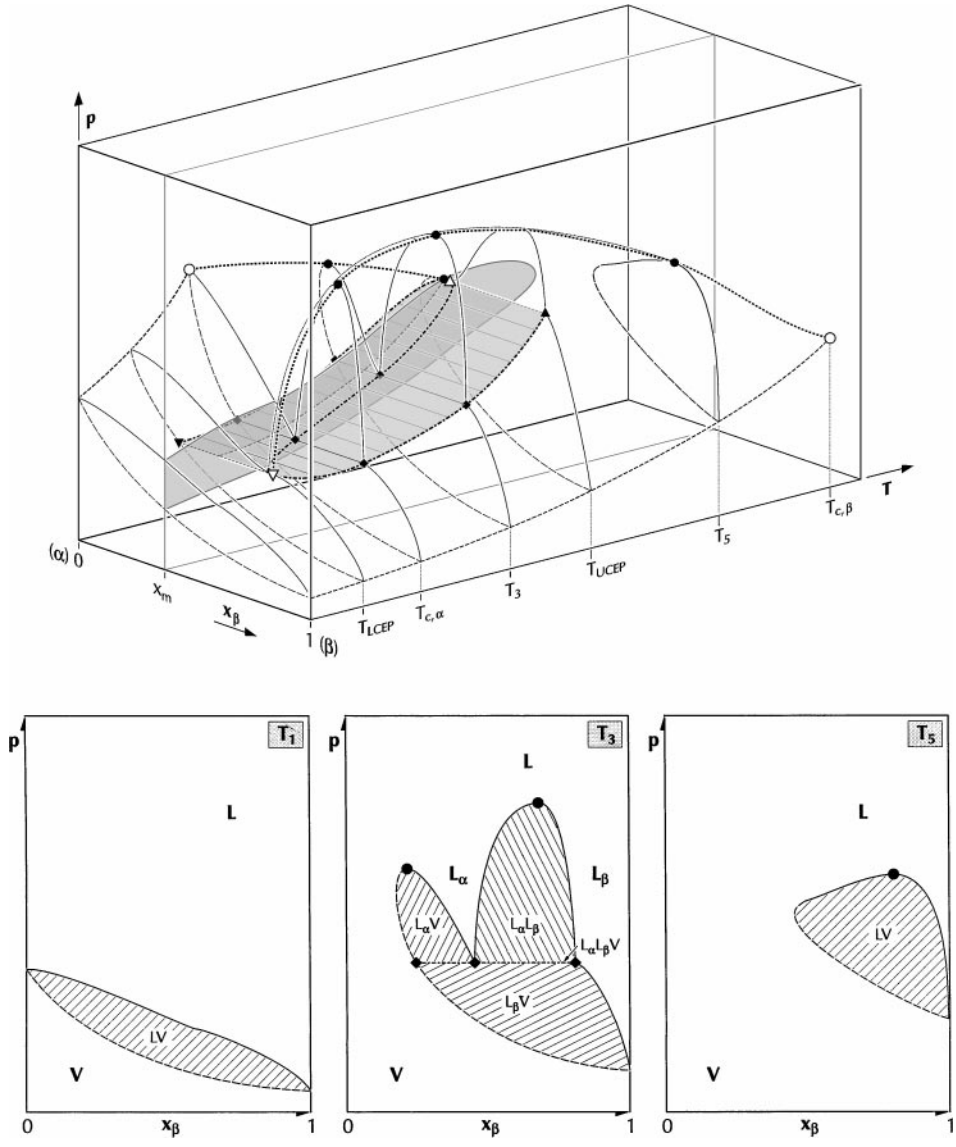

FIG. 11. Qualitative axonometry and corresponding intersections of the higher temperature section of a binary mixture conforming to type IV or V phase behavior. α: component of higher volatility; β: component of lower volatility; L: liquid phase; V: gaseous (vapor) phase; combinations of L, L_i, and V denote equilibria of mutually saturated phases and are emphasized by differing cross-hatched filling of the corresponding two-phase area. Full line (in intersections): bubble-point line; dashed line (in intersections): dew-point line; (○) critical point of the pure component; (●) mixture critical point (gas–liquid or liquid–liquid); (△) upper critical endpoint (UCEP); (▽) lower critical endpoint (LCEP); (◆) parameters of phases in equilibrium in $L_\alpha L_\beta V$ equilibrium shown in intersections. Note that the three-phase equilibrium $L_\alpha L_\beta V$ appears as a plane perpendicular to the p, T plane in p, T, x space. The isopleth at $x_\beta = x_m$ shows the same phase topology as found in the reaction mixture in the parameter range observed (see Fig. 12 right).

to increase with isothermal increase in pressure on the basis of both effects, as was experimentally observed in this study (Fig. 8). Above 80 bar, conversion strongly increased and reached its maximum with transformation of the mixture to a sc single-phase system, where PA can readily be hydrogenated without any mass transfer resistances caused by phase borders (4). In the single-phase region, however, conversion did not exhibit significant variation with pressure. This is interesting, since concentration of reactants and therefore residence time in the catalyst bed continued to increase as a consequence of the strongly increasing density with pressure. The apparently constant PA conversion in the single-phase region could be the result of the surface reaction or adsorption becoming the rate-limiting step or of possible deactivation due to the oligomer formation favored at higher pressure (density) (30).

The smooth change in the predominant phase of PA hydrogenation may also account for the observed decrease in selectivity with pressure (Fig. 8). Overhydrogenation of PA to EB is less likely in the liquid PA-rich phase due to the

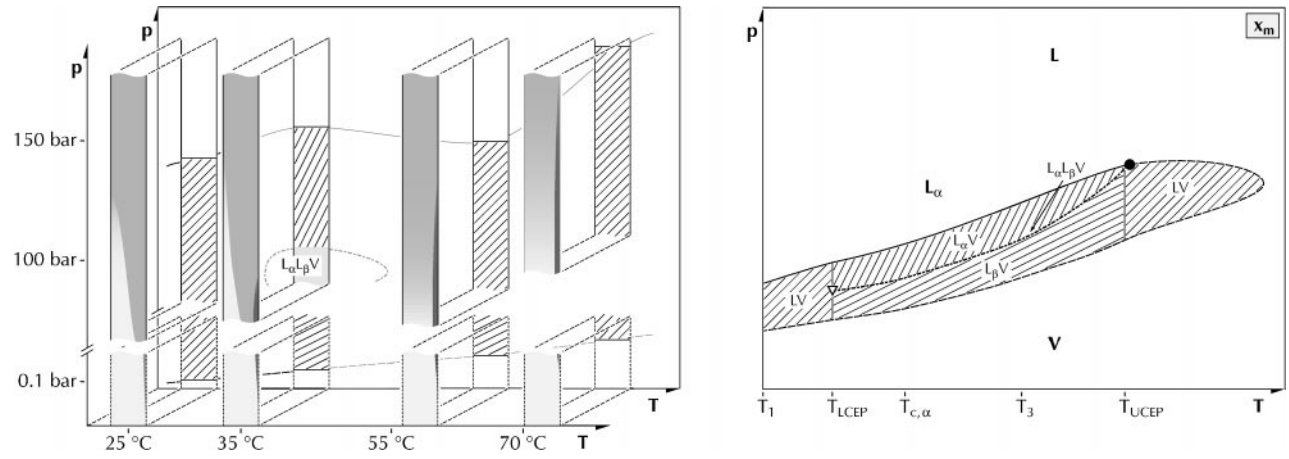

FIG. 12. Number and nature of phases in the hydrogenation mixture (left) and the isopleth at composition x_m in the binary phase diagram which are used to model the phase behavior of the reaction (right; for an axonometry of the phase diagram cf. Fig. 11). Note the similarity in phase behavior of the binary model and reaction mixture (cf. Fig. 6). The dew points for the reaction system (left) have been estimated on the basis of the vapor pressure of PA, calculated from a two-parameter corresponding states equation (32) using the ambient boiling point and the critical temperature and pressure (calculated in accord using the Ambrose method (32) as well as the Joback modification of Lyderson's method (32)) as references. For abbreviations and symbols cf. Fig. 11.

limited concentration of H_2 in this phase and, accordingly, on the catalyst surface (23). In the "sc" CO_2-rich phase, however, H_2 is readily available, facilitating overhydrogenation of PA. Since selectivity for consecutive reactions generally depends on conversion, the increase in conversion with pressure may also have a direct effect on selectivity. Both effects, the change in surface H_2 concentration and the increasing conversion of PA with overall density, would result in a decrease of selectivity with increasing pressure.

As a consequence of these tendencies, the optimum pressure range at a given temperature and hydrogen concentration is near the phase transition to a sc single-phase system at approximately 135 bar.

Concerning the influence of temperature at a given pressure of 127 bar and a $CO_2 : (PA : ST) : H_2$ molar ratio of $400 : (1 : 9) : 10$, the system exists first as a single phase at low temperatures and separates into a liquid PA–ST-rich phase and a dense CO_2-rich phase at higher temperatures. The still increasing conversion may be attributed to a dramatic increase of the reaction rate in the liquid (and presumably also in the gaseous) phase, which overcompensates for the negative effect of separation into two phases, as was discussed previously. The appearance of a maximum in selectivity might be due to different ratios of reaction rates for the hydrogenation of PA and of ST (Scheme 1) in the various phases.

Finally, at increased $H_2 : CO_2$ ratios a much higher pressure is needed to reach the density required for complete miscibility of PA–ST in CO_2. Consequently, for increasing hydrogen concentrations at a given pressure (127 bar) and temperature (55°C), separation into a liquid PA–ST-rich phase and a dense CO_2-rich phase is expected, but was found to be detrimental to PA conversion in the pressure experiment. Nevertheless, conversion increases, which must be attributed to a strong influence of the hydrogen concentration on the reaction rate. On the other hand, higher hydrogen concentrations favor overhydrogenation to EB, leading to the observed steady decrease in selectivity. Both effects lead to the conclusion that the hydrogen excess should be kept as low as possible in order to gain high styrene purity.

After the H_2 concentration in the CO_2/PA–ST/H_2 mixture is lowered so that single-phase conditions are reached, an optimum hydrogen amount might be identified in the single-phase region, so that both conversion and selectivity are high. The lower optimum hydrogen concentration found for the single-phase system, however, will be far from ideal for hydrogenations in a multiphase system. In fact, conducting the reaction at a high hydrogen excess—and thus, at moderate densities, in a two-phase system—will most probably lead to a much higher "best" hydrogen concentration upon optimization of the reaction conditions, since the solubility of hydrogen in the liquid phase and the mass transport resistances limit the hydrogen concentration at the catalyst surface. These apparently "ideal" conditions at high hydrogen concentrations, however, may only represent a local optimum.

The generally high activity and selectivity observed for the amorphous metal alloy catalyst in the semihydrogenation of PA are traced to the unique chemical structure of its surface, its nonporosity (avoiding pore diffusion), and its excellent heat conduction, due to its metallic properties (15).

The combination of this highly active catalyst with the good mass transfer properties of the reaction medium

(single-phase region) facilitates efficient application of a continuous fixed-bed reactor. Single-phase conditions have been suggested to be beneficial for fat hardening; however, the existence of single-phase behavior has not not been confirmed by specific phase behavior studies (31). To identify the single-phase conditions, consideration of the phase behavior is imperative and must be taken into account when catalytic data are interpreted.

Comparison to batch experiments, performed in an autoclave under identical conditions, confirmed that similarly high or even higher selectivities at comparable conversion could be achieved at a superior ST production per reactor volume in the flow reactor setup. Due to the significantly smaller volume compared to the often employed batch system (autoclave), the flow reactor additionally bears a reduced risk potential for reactions at elevated pressures and offers advantages in sustaining isothermal conditions, which is particularly important for Lindlar-type reactions. Furthermore, it allows facile integration into a multistep process on an industrial scale and makes possible fully automated operation, including easy separation of the product stream and recycling of the solvent. All together this constitutes a significant step toward the development of a "green" process.

CONCLUSIONS

The semihydrogenation of phenylacetylene over an amorphous $Pd_{81}Si_{19}$ metal alloy at elevated pressures, employing sc CO_2 as a solvent, was investigated. High conversion and selectivity were achieved over this catalyst without chemical modification, usually applied for Lindlar-type catalysts. In the parameter range examined, complex phase behavior, including several phase transitions, was observed. Hydrogenation of PA to ST yielded the highest conversions and good selectivities at the edge of the sc single-phase region. In order to reach the density necessary for complete miscibility of the reactants in CO_2 at reasonable pressures, both temperature and hydrogen excess must be kept low. Moreover, excess hydrogen in the system leads to overhydrogenation of PA and thus to a steady decrease in selectivity. A one-phase system with low hydrogen excess appears to be an ideal reaction medium for such hydrogenations, due to the enhanced mass transfer properties under these conditions and a more precise reaction control.

The use of an amorphous palladium–silicon metal alloy catalyst under "supercritical" conditions represents a novel and promising route for this type of semihydrogenation, as current studies with other substrates corroborate. Linking phase behavior studies and catalytic investigations seems to be a necessary prerequisite for optimizing operation conditions of this advanced process design.

ACKNOWLEDGMENTS

We thank Thomas Bürgi for performing the XPS investigations. Financial support by the Swiss "Bundesamt für Energie" (BFE) and the Swiss "Kommission für Technologie und Innovation" (KTI), as well as Degussa AG and F. Hoffmann-La Roche AG, is gratefully acknowledged.

REFERENCES

1. Jessop, P. G., Ikariya, T., and Noyori, R., *Chem. Rev.* **99**, 475 (1999).
2. Brennecke, J. F., and Chateauneuf, J. E., *Chem. Rev.* **99**, 433 (1999).
3. Jessop, P. G., and Leitner, W. (Eds.),"Chemical Synthesis Using Supercritical Fluids." Wiley–VCH, Weinheim, 1999.
4. Baiker, A., *Chem. Rev.* **99**, 453 (1999).
5. Savage, P. E., *in* "Handbook of Heterogeneous Catalysis" (G. Ertl, H. Knözinger, and J. Weitkamp, Eds.), Vol., 3 p. 1339. Wiley–VCH, Weinheim, 1997.
6. Leitner, W., *Appl. Organometal. Chem.* **14**, 809 (2000).
7. Baiker, A., *Appl. Organometal. Chem.* **14**, 751 (2000).
8. Ambrose, D., *in* "Handbook of Chemistry and Physics" (D. R. Lide, Ed.), p. 6. CRC Press, Boca Raton, FL, 1991.
9. Hitzler, M. G., Smail, F. R., Ross, S. K., and Poliakoff, M., *Org. Process Res. Dev.* **2**, 137 (1998).
10. Butler, J. R., and Kelly, K. P., EP European Patent EP584054A1, 1994.
11. Matsui, T., and Morimoto, H., *Kagaku Kogaku Ronbunshu* **22**, 512 (1996).
12. Priddy, D. B., and Roe, J. M., U.S. Patent 4389517, 1983.
13. Molnar, A., Smith, G. V., and Bartok, M., *J. Catal.* **101**, 67 (1986).
14. Molnar, A., Smith, G. V., and Bartok, M., *Advan. Catal.* **36**, 329 (1989).
15. Baiker, A., *in* "Glassy Metals III," Vol. 72, p. 121. Springer-Verlag, Berlin, 1994.
16. Baiker, A., *in* "Handbook of Heterogeneous Catalysis" (G. Ertl, H. Knözinger, and J. Weitkamp, Eds.), Vol. 2, p. 803. Wiley–VCH, Weinheim, 1997.
17. Dhamodharan, R., *Chem. Lett.* 235 (1996).
18. Rajaram, J., Narula, A. P. S., Chawla, H. P. S., and Dev, S., *Tetrahedron* **39**, 2315 (1983).
19. Wagner, C. D., Davis, L. E., Zeller, M. V., Taylor, J. A., Raymond, R. M., and Gale, L. H., *Surf. Interface Anal.* **3**, 211 (1981).
20. Wandeler, R., Künzle, N., Schneider, M. S., Mallat, T., and Baiker, A., *J. Catal.* **200**, 377 (2001).
21. King, M. B., "Phase Equilibrium in Mixtures." Pergamon, Oxford, 1969.
22. Rowlinson, J. S., and Swinton, F. L., "Liquids and Liquid Mixtures," 3rd ed. Butterworth, London, 1982.
23. van der Aalst, M. J. M., and Benito, F. A., U.S. Patent 5504268, 1996.
24. Maurer, B. R., and Galubardes, M., U.S. Patent 4822936, 1989.
25. Noack, K., Rehren, C., Zbinden, H., and Schlögl, R., *Langmuir* **11**, 2018 (1995).
26. Chrastil, J., *J. Phys. Chem.* **86**, 3016 (1982).
27. Scott, R. L., and van Konynenburg, P. H., *Discuss. Faraday Soc.* **49**, 87 (1970).
28. van Konynenburg, P. H., and Scott, R. L., *Philos. Trans. Roy. Soc. London Ser. A* **298**, 495 (1980).
29. Esteruelas, M. A., Gonzalez, I., Herrero, J., and Oro, L. A., *J. Organomet. Chem.* **551**, 49 (1998).
30. Tschan, R., Wandeler, R., Schneider, M. S., Burgener, M., Schubert, M. M., and Baiker, A., *Appl. Catal. A*, in press.
31. van den Hark, S., and Harrod, M., *Appl. Catal. A* **210**, 207 (2001).
32. Reid, R. C., Prausnitz, J. M., and Poling, B. E., "The Properties of Gases and Liquids," 4th ed. McGraw–Hill, New York, 1988.